



Intermittent beading in fiber composites

Israel Greenfeld^{*},¹, Wenyong Zhang¹, XiaoMeng Sui, H. Daniel Wagner^{**}

Department of Materials and Interfaces, Weizmann Institute of Science, Rehovot 76100, Israel

ARTICLE INFO

Article history:

Received 5 September 2017

Received in revised form

7 January 2018

Accepted 3 March 2018

Available online 7 March 2018

Keywords:

Composite

Fiber reinforcement

Interface

Intermittent beading

Fragmentation

Pullout

ABSTRACT

Simultaneous improvement of strength and toughness is a challenge in composite materials, as an improvement in one is generally at the expense of the other. The filler-matrix interface has a crucial role in such improvement. It appears that modification of the interfacial structure/geometry may have wider possibilities and benefits than the classical chemical bonding approach. Using a model glass-epoxy fiber-reinforced composite, we modified the regular cylindrical fiber-matrix interface by applying intermittent epoxy beads along the fiber, taking advantage of the Plateau-Rayleigh liquid instability phenomenon. Under load, the beads serve as fiber anchors in the matrix, thus exploiting the fiber strength to its maximum. During fracture, the pullout of beads through the matrix appears to dissipate more plastic deformation energy compared to the pullout of regular fibers. Fragmentation tests of beaded fibers in epoxy matrix demonstrate these failure mechanisms; single-bead fiber pullout tests with different bead sizes and surface treatments provide strength and toughness data that substantiate this approach. The concept of intermittent beading has ample possibilities for optimization. It is also scalable and therefore practical.

© 2018 Elsevier Ltd. All rights reserved.

1. Background and motivation

Engineering materials are designed to be either strong or tough, but rarely both simultaneously. Indeed, strength and toughness often do not co-exist, and the design of strong and tough materials is inevitably a compromise [1–4]. For example, engineering ceramics are much stronger than metal alloys but their toughness is much lower because they are brittle [5]. While the strongest materials gain their strength from covalent bonds in their crystalline structure, the breaking of these bonds during fracture does not absorb much energy, and even a nanoscale flaw can initiate crack propagation leading to failure [6]. Tough materials, on the other hand, rely on complex energy absorbing mechanisms, such as rearrangement of molecules by plastic deformation and chain mobility in polymers. Structural design strategies at the molecular level can sometimes resolve this strength-toughness conflict. For example, the flow-induced molecular orientation in electrospun polymeric nanofibers yields simultaneous improvement in both strength and toughness [7–9].

Tuning the filler-matrix interface plays a crucial role in the mechanical properties of composites, but in many cases an improvement in strength is accompanied by a degradation in toughness, and vice versa. Here again, structural design strategies often resolve this conflict, and examples from nature abound, including teeth, wood, bones, shells, sponge spicules and tendons [10]. Bone is a hierarchical composite, self-assembled through seven levels from nanoscale to macroscale, achieving low weight and balanced strength and toughness [11]. Similarly, the exceptional mechanical properties of bamboo originate from its multi-level structure that consists of strong fibrils and soft matrix at different scales and graded densities [12]. A recently developed multilevel structure using carbon nanotube fibers (CNTF) impregnated by a soft interphase promises similar benefits [13,14].

In the case of fiber-reinforced composites, which are the subject of the current study, the fiber-matrix interface must be strong enough to ensure stress transfer to the fibers, leading to overall strength, but weak enough to enable plastic deformation of the interfacial layer, so as to dissipate energy and redistribute stresses around defects and cracks. Toughness is achieved by energy absorption as a result of the formation of new crack surfaces, fiber debonding, interfacial friction, fiber breaking, fiber pullout, and crack bridging by unbroken fibers [15]. A major toughening mechanism is matrix yielding and plastic flow caused by the pullout of fibers from the matrix during fracture [13,16]. The classic

^{*} Corresponding author.

^{**} Corresponding author.

E-mail addresses: green_is@netvision.net.il (I. Greenfeld), Daniel.Wagner@weizmann.ac.il (H.D. Wagner).

¹ These authors contributed equally to this work.

Cottrell-Kelly-Tyson (CKT) model [13,17–19] describes the composite toughness and strength.

The overall performance improvement achievable by chemically tuning the interfacial strength is somewhat limited and may lead to undesired degradation of either strength or toughness. Two approaches, which focused on topological obstacles at the interface rather than on its chemical nature, were suggested as alternatives. The first, termed intermittent bonding (Fig. 1b) or hybrid sizing, was suggested by Atkins [20,21] and Jensen et al. [22,23]. The second, termed bone-shaped fibers (Fig. 1a) or fibers with enlarged ends, was suggested by Phanthien [24,25], Zhu et al. [26–30], and Wetherhold et al. [31–34]. In intermittent bonding, long fibers have alternate sections of high and low adhesion (that is, interfacial shear strength), obtained by periodic surface treatments, resulting in a significant improvement in toughness at only a mild degradation in strength. In bone-shaped fibers, the ends of short fibers made of ductile thermoplastic polymer or metal are enlarged, resulting in anchoring and improved strength and fracture toughness. An approximately similar configuration is observed in nature, in the dovetail shape of the ceramic platelets that reinforce nacre [35]. Another analogy can be seen in ribbed steel rebars (reinforcing bars) used to enhance concrete gripping in construction. Interestingly, shape modulation of carbon fibers using lasers was recently suggested by Blaker et al. [36], but with very small taper angles.

Here, we propose a new conceptual approach, *intermittent beading* (Fig. 1c), whereby multiple beads are applied on a fiber which is then embedded in a matrix for the purpose of composite reinforcement. Stress transmission from the matrix to the fiber is achieved mainly through the bead, instead of directly from matrix to fiber. The use of a single polymer bead on a fiber is common in micro-droplet debonding tests [37–39]. Intermittent beading is, however, completely different in its function and structure: it aims to resolve the shortcomings of intermittent bonding and bone-shaped fibers, specifically, the reduction in composite strength in the former and the relevance only to short and ductile fibers in the latter. Considering that long fibers are generally favored over short ones in terms of mechanical performance as well as ease of handling and alignment, intermittent beading has the potential to improve the toughness of composites reinforced with long fibers by dissipating energy through pullout of beads from the matrix. Intermittent beading can also potentially improve the strength thanks to its strong intermittent topological anchors (beads), which securely lock the fiber in the matrix.

As a convenient model for this study, we used glass fibers with epoxy beads, uncoated or coated with a release agent and embedded in epoxy matrix. Results of pullout, fragmentation, and compact tension tests, and performance assessment of a composite reinforced by beaded fibers, are presented and discussed. We

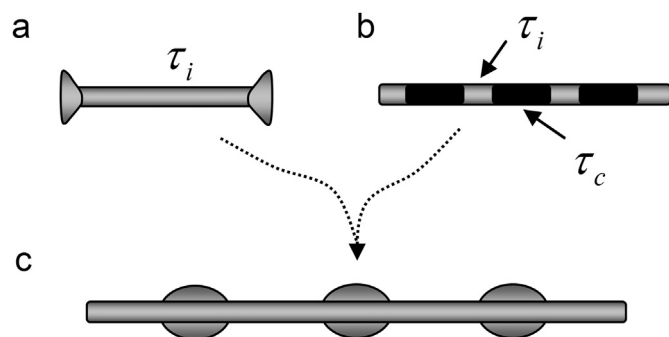


Fig. 1. Intermittent beading concept. (a) Bone-shaped fiber. τ_i is the fiber-matrix interfacial strength. (b) Intermittent bonding fiber. τ_c is the interfacial strength of the coated sections. (c) Intermittent beading fiber.

confined ourselves in this basic composites research to unidirectional alignment of long beaded fibers, with loading in the fibers direction, and to the CKT approach in the analysis of the composite strength and toughness.

2. Experimental

2.1. Materials

The E-glass fibers were first rinsed in acetone several times and dried at 80 °C for 1 h to remove surface impurities. The epoxy resin used in this study for both the matrix and the beads was a mixture of bisphenol-A diglycidyl ether (EP828, epoxy resin, Polymer Gvulot Ltd.) and polyetheramine (EPC 304, epoxy hardener, Polymer Gvulot Ltd.), with a weight ratio of 100:42, degassed for 60 min. The curing schedule of the epoxy resin was 100 °C for 6 h. Three types of fibers were used: pure E-glass fiber (denoted F, used as reference, $d \cong 18 \mu\text{m}$), beaded glass fiber (denoted FB), and coated beaded glass fiber (denoted FBC). The coating was a commercial epoxy release agent (MR571/A-64, Skiba Ltd.), based on a blend of natural and synthetic polymers.

2.2. End-beaded fibers

The fibers were spanned on a shelf with a slight tension (about 0.5 g) to straighten them. Then, a copper wire ($d = 20 \mu\text{m}$) was used to deposit a small amount of liquid epoxy resin, degassed for 30 min, on the spanned single fibers. Under the effect of surface tension, the resin formed into a curved bead, the shape of which is described in detail in Supporting Information S2. To produce a sufficient quantity of specimens, many beads were deposited on a single fiber at about 5 mm spacing. The beaded fiber was subsequently degassed again for 30 min and cured at 100 °C for 6 h. Finally, under an optical microscope, the fiber was cut into short segments by a scalpel, leaving a bead at one end of each segment and a free fiber section at the other end. The diameter of the bead on each fiber segment was measured by optical microscopy, and only flawless beads were used for testing. For coating, the beaded fiber was dipped in the release agent several times, creating a very thin layer on the bead and on the free section of the fiber.

2.3. Multiple beaded fibers

Multiple beads were created by applying the epoxy resin on a glass fiber, exploiting the Plateau-Rayleigh instability phenomenon [40]. The instability, first explained by Plateau [41] and Lord Rayleigh [42] in 1873, causes spontaneous partitioning of a liquid cylindrical film into (approximately) evenly spaced drops (Fig. 2). The instability phenomenon is described in detail in Supporting Information S1.

A single E-glass fiber without any surface treatment was vertically suspended, and a drop of liquid epoxy resin, degassed for 30 min, was deposited on the fiber top. As the viscous resin slid downward the fiber, a uniform epoxy layer was formed. Because of the liquid instability, the epoxy layer quickly separated into a string of drops, leaving a thin epoxy film on the free fiber sections. The resulting fiber with the epoxy beads was degassed again for 30 min and cured at 100 °C for 6 h. For coating, the beaded fiber was dipped in the release agent several times, creating a very thin layer on the beads and on the free sections of the fiber.

2.4. Pullout sample and testing

Once an end-beaded fiber was prepared, the end without bead was fastened to a homemade assembly composed of two

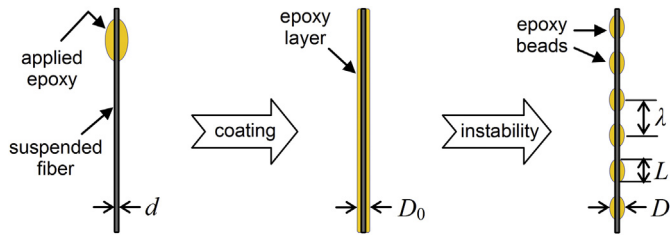


Fig. 2. Preparation of intermittent beading on fibers. A fiber of diameter d is coated by a liquid epoxy layer D_0 , which spontaneously breaks into evenly spaced beads at wavelength λ as a result of the Plateau-Rayleigh instability.

orthogonal microcallipers, a rotating platform and a heating device (Fig. 3a). Under the fastened fiber, a screw whose cap was filled with liquid epoxy resin (depth of 5 mm) was vertically installed on the heating device. The components of the epoxy resin, the degassing and the curing process were the same as those of the epoxy beads. By adjusting the microcallipers and the rotating platform, the beaded end could be vertically embedded in the epoxy resin at a desired depth. The heating device was then turned on to 100°C for 1 h to partially cure the epoxy so as to fix the position of the beaded fiber in the screw. Finally, the screw together with the embedded fiber was placed in an oven at 100°C for an additional 5 h to complete the curing process. Because of epoxy shrinkage during curing (the liquid level declined by about $20\ \mu\text{m}$ after curing), the initial embedding depth was set $20\ \mu\text{m}$ deeper than the desired value.

The embedded length was $L_e = 120\ \mu\text{m}$, and the free length of the fiber was $30\text{--}50\ \mu\text{m}$. The bead length was $L \cong 80\text{--}90\ \mu\text{m}$ and its diameter was $D \cong 40\text{--}50\ \mu\text{m}$. Note that in a beaded fiber, the embedded length is the fiber length inside the bead plus the remaining fiber length in the matrix (Fig. 3b). The embedded length is about half the beads wavelength, emulating a realistic composite failure scenario when the matrix fracture plane is in-between two beads. When release agent coating was applied, it covered both the bead and the thin epoxy film on the fiber free section, and provided reduced bead-matrix and fiber-matrix bonding strength and friction. At least 5 specimens were tested for each fiber configuration (F, FB and FBC), with and without release agent.

The pullout of the embedded fiber was performed on a homemade assembly with a piezo actuator and a high voltage amplifier (Physik Instrumente GmbH, Germany) (Fig. 3b). The measuring range of the load cell (Kistler Type 9207, Switzerland) was -50 to

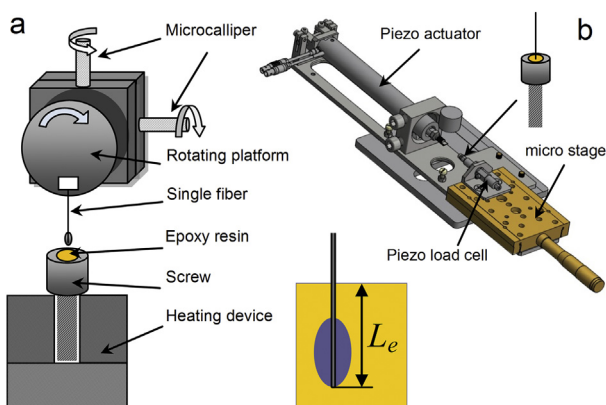


Fig. 3. Pullout sample preparation and testing devices. (a) Embedding device, used for inserting a beaded fiber in epoxy resin at a desired embedded depth L_e , and fixing its position by heating. (b) Pullout device, used for pullout testing of an embedded beaded fiber.

50 N, and the crosshead movement range was $180\ \mu\text{m}$ with a constant speed of $1\ \mu\text{m/s}$. The screw with the embedded fiber was threaded into a mating socket in the load cell. The fiber free end was glued onto a horizontal steel strip attached to the crosshead. All components of the apparatus were designed to have high stiffness. The setup was mounted on an optical microscope to monitor the test and record the experiment by a digital camera. The test was controlled by the software developed specifically for this device (Federal Institute for Materials Research and Testing (BAM), Berlin) including drift compensation of the piezo components, and the load/displacement data was recorded and presented.

2.5. Fragmentation sample and testing

Once a multiple beaded fiber was prepared, it was embedded in a dumbbell specimen with a cross-section of $1 \times 0.8\ \text{mm}^2$ and a gauge length of 12 mm (Fig. 4a). The components of the epoxy resin, the degassing and the curing process were the same as those of the epoxy beads. Two groups of reinforced specimens were prepared, single fiber and fiber mini-bundle. The mini-bundle consisted of 10 fibers, spaced at $50\ \mu\text{m}$ intervals and arranged in two rows.

The fragmentation tests were performed on a Minimat tensile test instrument equipped with a 200 N load cell, at a displacement rate of $50\ \mu\text{m/min}$. The stress distribution in the transparent epoxy medium was monitored by a polarizing optical microscope (POM, Nikon) (Fig. 4b–d) and recorded by a video camera attached to it (Supporting Information fragmentation video). The field of view of the camera lens covered the central part of the specimen. The video and the test were synchronized, so that the stress level and fiber breaks could be correlated. Because of the observed complex fracture phenomena of the fiber-bead-matrix system, the usual fragmentation saturation and break counting could not be reliably detected and measured, and therefore the test analysis was mostly qualitative. At least 8 specimens were tested for each fiber configuration (F, FB and FBC).

Supplementary video related to this article can be found at <https://doi.org/10.1016/j.compscitech.2018.03.003>.

2.6. Optical and electron microscopies

The formations of beads on the fiber were viewed and measured by optical microscopy (OM) and scanning electron microscopy (SEM). The thickness of the thin film covering the fiber sections

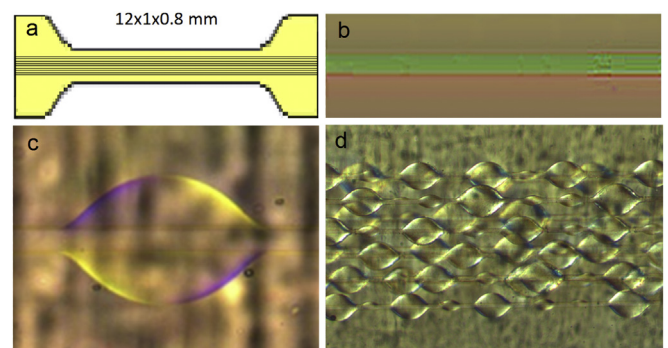


Fig. 4. Fragmentation test sample and microscopy. (a) Dumbbell specimen with fiber bundle for tensile tests. (b–d) Birefringence images viewed by a polarized optical microscope, showing the highly stressed regions in the epoxy (in color) in a beadless fiber (b), a beaded fiber (c), and a bundle of ten beaded fibers (d). (For interpretation of the references to color in this figure legend, the reader is referred to the Web version of this article.)

outside the beads was measured by SEM on a beaded fiber broken by a tensile test. Pulled out beadless and beaded fibers, and the respective exit holes in the matrix, were probed by SEM. The fracture surfaces of fibers and beads broken during the fragmentation tests were probed by SEM.

3. Results and discussion

3.1. Intermittent beading

Typical shapes of beads after forming through the Plateau-Rayleigh liquid instability and curing are presented in Fig. 5. The beads appear to be smooth and evenly spaced (Fig. 5a and b), with diverse sizes and aspect ratios (Fig. 5c). A thin epoxy film of 100–200 nm thickness is seen on the fiber surface between beads (Fig. 5b), the consequence of the steep slowing down of the flow rate when the liquid film becomes thin, allowing enough time for the epoxy to cure (Supporting Information S1). At times, the bead size alternates between small and large (Fig. 5d), originating from a secondary instability that forms small drops in the liquid sheath between larger drops [40].

The measured wavelength λ (the distance between bead centers) and bead length L are plotted against the beads diameter D (Fig. 6), and compare well with the theoretical predictions (Supporting Information S3) for a liquid-fiber contact angle of $\theta_E = 15^\circ$.

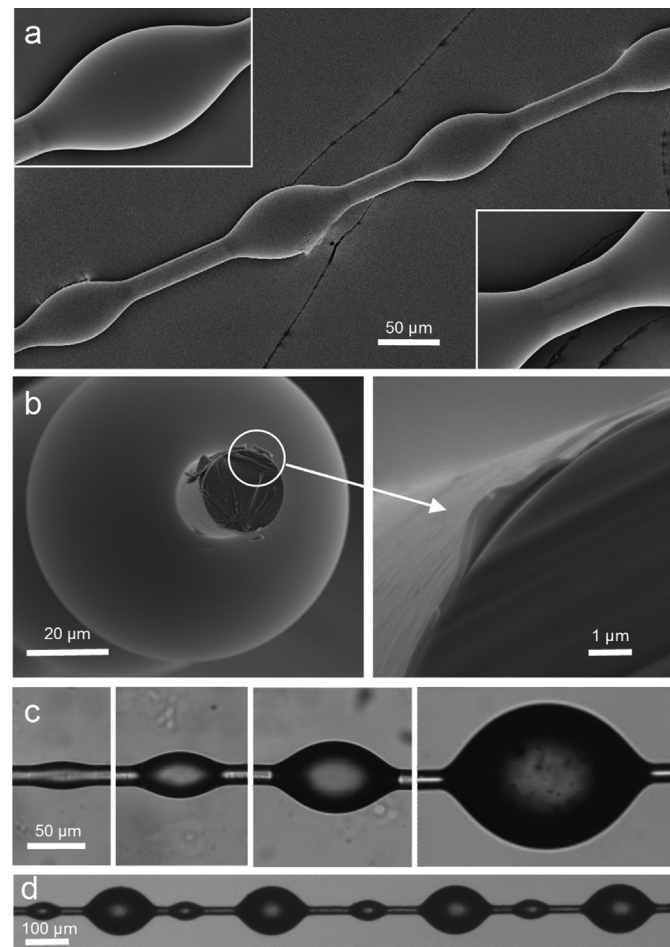


Fig. 5. Cured EP-828 epoxy beads formed on 18 μm E-glass fibers. (a) SEM images of beads. (b) SEM images of a beaded fiber, broken after tensile test. Magnification shows thin coating film of thickness 100–200 nm between beads. (c) OM images of beads of different sizes. (d) Alternating large and small beads on a fiber.

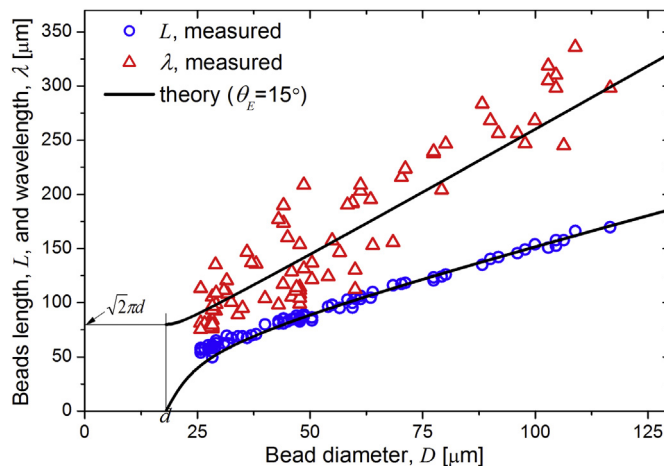


Fig. 6. Beads size and frequency. Measured diameter, length and wavelength of Epoxy EP-828 cured beads on E-glass fibers of diameter $d = 18 \mu\text{m}$, and comparison to theoretical simulation for contact angle $\theta_E = 15^\circ$.

15° . The bead diameters varied from 25 to 120 μm , and the corresponding lengths and wavelengths varied from 50 to 170 μm and from 70 to 330 μm , respectively. Within the size range of our study, the following linear fits were found useful ($R^2 > 0.97$): $L_{\mu\text{m}} \cong 24.6 + 1.27D_{\mu\text{m}}$ and $\lambda_{\mu\text{m}} \cong 1.73L_{\mu\text{m}}$. The varying bead sizes and wavelengths observed in Fig. 6 are the result of different liquid coating thicknesses used in samples preparation. The liquid coating layer on the fiber could not be measured, as the beads formed almost instantaneously. However, using the theoretical relationship between the beads wavelength and the liquid coating diameter, $\lambda = \sqrt{2\pi D_0}$ [40,43] (Supporting Information S3), the range of coating thicknesses used in the study can be assessed as from about 1 μm up to about 25 μm .

By (theoretically) varying the liquid coating thickness and the liquid-fiber contact angle, a variety of bead shapes, sizes and frequencies can be obtained (Supporting Information S2–S3). A useful prediction for bead diameters when the coating diameter is large compared to the fiber diameter ($D_0 \gg d$) is given by $D \cong 1.88D_0$. An important concern about the technique is whether gravity can adversely affect the beads shape and frequency. However, as shown in Supporting Information S1, the effect of gravity can be neglected because surface tension is dominant over gravity in micro-scale drops. Another important consideration when applying the technique is how fast do the drops form, particularly in view of the high sensitivity of the formation time to the liquid coating thickness, such that large drops form much faster than small ones. However, as shown in Supporting Information S1, for typical coating thicknesses of several microns or higher, the drops formation time should be typically less than 1 s, making this beading method a practical technique for engineering applications.

3.2. Single bead on a fiber - pullout tests

Pullout tests were conducted to investigate the effects of beading and coating on the fiber pullout strength and work. Examples of pullout events of beaded fibers are shown in Fig. 7. Without coating, the fiber typically breaks inside the bead, then pulls out from it (Fig. 7a), while the bead remains embedded inside the matrix but causes an observable plastic deformation around the exit hole (Fig. 7d). By contrast, when coated, the fiber typically pulls out with its bead still attached (Fig. 7b), as evidenced by the large exit hole in Fig. 7e.

Fig. 7b is particularly interesting, as it demonstrates that the

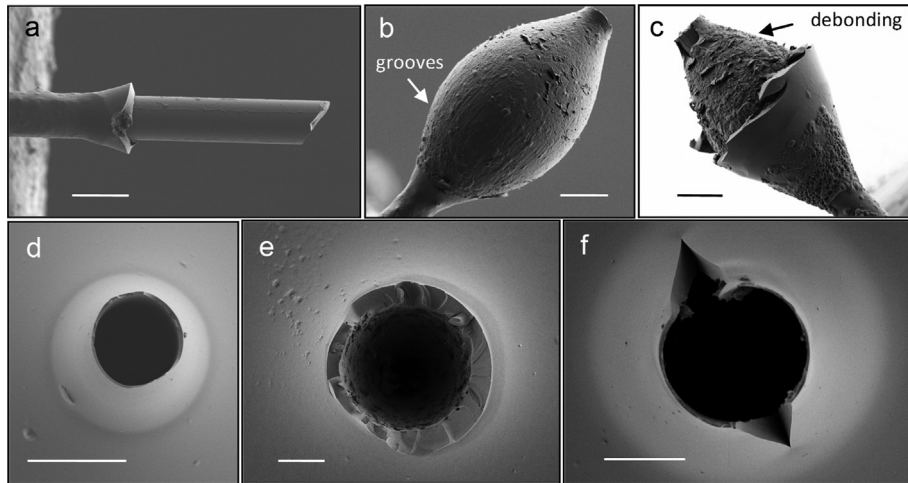


Fig. 7. SEM images of beaded fiber and matrix after pullout. 18 μm E-glass fiber with single EP-828 epoxy bead, without coating (a,d) and with coating (b,c,e,f). All scale bars are 20 μm . (a) Fiber pulled out from bead. (b) Pulled out bead, with groove marks at bottom and debonding marks at top. (c) Pulled out, partially peeled-off bead. (d) Bulging deformation of exit hole, bead remained embedded. (e) Large exit hole after bead pullout. (f) Large cracked exit hole after bead pullout.

fracture process involves debonding of the bead from the matrix on the side where the interface is under tension (the upper-right side on the picture), followed by plastic deformation of the matrix on the side pressing against the matrix, as evidenced by the parallel groove marks on the bead. In some cases, the bead remained bonded to the fiber but its outer boundary was partially peeled off due to debonding (Fig. 7c), and in others cracks appeared in the bead's exit hole (Fig. 7f). We conclude that the anchoring mechanism of the bead is effective in both coated and uncoated fibers. Furthermore, coating seems to be advantageous by easing bead pullout and avoiding premature fiber breakage, thus likely dissipating considerable plastic energy.

These qualitative observations are substantiated by measurements of the pullout force (the force applied at the fiber free end) and work (the total work invested in pulling out). The force-displacement plots of typical pullout tests (Fig. 8a) and the maximum force plots (Fig. 8b) show higher pullout forces and longer plastic displacements in beaded fibers compared to beadless fibers. Coating further increases the force and the total displacement, and is accompanied by some reduction in stiffness (lower force-displacement slope). As a result, the pullout work of beaded fibers is higher compared to beadless fibers, with a dramatic increase for coated fibers (Fig. 8c).

The pullout force and work of beaded fibers are strongly dependent on the bead size (Fig. 8d and e). A larger bead requires a higher pullout force, and dissipates more energy when pulled out. The rise of the pullout force and work with respect to bead size seems exponential. Evidently, there should be a limit to bead size (not reached in the coated samples of the current study), because at a certain critical size the bead's mechanical locking force will exceed the fiber strength or the fiber-bead bonding strength. This is further clarified later on.

These results substantiate the benefit of beaded fibers and their likely contribution to both the composite strength and toughness. Somewhat surprisingly, the coating of beaded fibers improves (increases) their pullout strength. This is attributed to the different stress distribution in the fiber-bead-matrix system, which appears to favor bead pullout over fiber breakage and pullout, at the expense of a somewhat lower stiffness, as clarified later on by the discussion on the bead locking mechanism. Beaded fibers appear to provide a more stable pullout force compared to the wider dispersion of values in beadless fibers (Fig. 8a and b), most likely because their locking mechanism is not as sensitive to bonding quality.

3.3. Multiple beads on a fiber - fragmentation tests

Tensile tests were conducted with coated and uncoated beaded single-fiber composite specimens to investigate (i) the stress distribution in the epoxy in and around the beads, and (ii) the failure mechanisms of intermittent beading in a representative structure. Under increasing tensile load, such single-fiber composite tests usually lead to fiber fragmentation, whereby the embedded fiber progressively breaks into smaller fragments until a saturation limit is reached. This saturation length is then used to evaluate fiber-matrix interfacial adhesion and the ability of the interface to transfer shear stresses, via a parameter classically termed the critical fiber length (l_c). It is also of interest to examine how the presence and characteristics of beads (including their frequency, shape, size) affect the fragmentation phenomenon and the fracture process in general. This interesting issue is discussed here. Examples of fragmentation events of beaded fibers are shown in Fig. 9 and in the Supporting Information fragmentation video.

Generally, the fragmentation process is seen to span several stages, as described ahead, not always in the same sequence. First, beads debond from the matrix from one or both sides (Fig. 9a–c), as a result of tension caused by the higher elongation of the matrix with respect to the fiber. Then, debonding continues to propagate along the fiber in-between beads, and the fiber eventually breaks at highly stressed regions, releasing fiber tension and causing the beads to press against the matrix in opposite directions (Fig. 9d). As the external load is further increased and more fiber sections break, recurrent pairs of beads still connected by highly stressed fiber segments is observed (Fig. 9e), whereas between the pairs the fiber is broken and the stress is relieved. The surfaces of beads previously under compression push against the matrix and plastically deform it into elongated cavities (Fig. 9f). The plastic distortion is substantial and the resulting displacement is much longer than observed in the pullout tests (Fig. 8a), implying that matrix fracture is delayed when the beads are completely surrounded by matrix.

Further on, the fiber breaks progressively into smaller fragments at several locations, generating gradually propagating cracks in the matrix (Fig. 9g and h). Eventually, the matrix breaks, and beaded fibers are pulled out from the matrix through the fracture surfaces (Fig. 9i and j). In uncoated samples, debonding occurs between the fiber and bead rather than between the bead and matrix, and plastic deformation of the matrix by the bead is present but less pronounced.

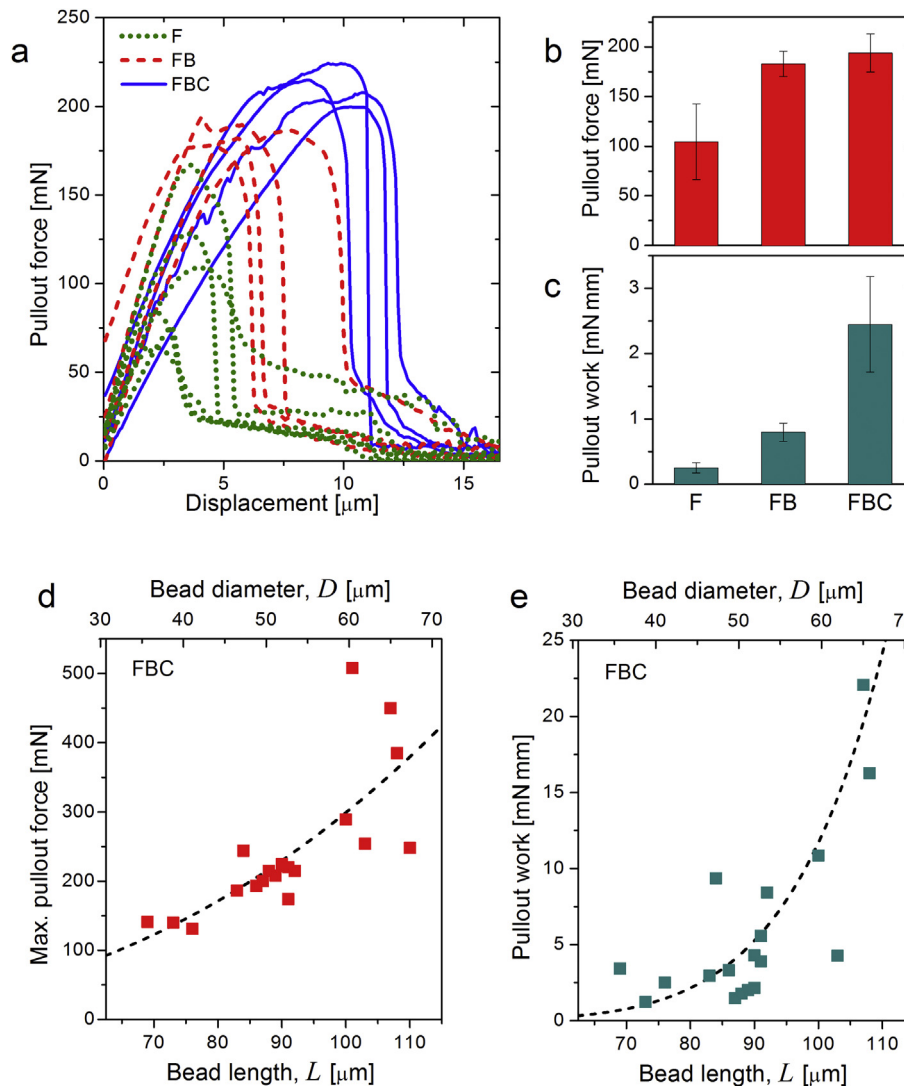


Fig. 8. Pullout force and work. 18 μm E-glass fiber with single EP-828 epoxy bead, embedded at length of 120 μm . Bead length and diameter were 80–90 μm and 40–50 μm , respectively, unless otherwise stated. (a) Typical pullout force vs. displacement, for fibers (F), fibers with beads (FB), and fibers with coated beads (FBC). (b) Average maximum pullout force for the three configurations (F, FB and FBC). (c) Average pullout work (area under the force-displacement plot) for the three configurations. (d) Average maximum pullout force and (e) average pullout work vs. bead length and diameter for coated beaded fibers (FBC). Dashed lines indicate trends.

Matrix cracks can nucleate inside or outside beads (Fig. 9g), typically as a result of a fractured fiber, and consequently specimen fractures run through a free fiber section or through a beaded section. In uncoated samples, fiber breaks usually initiate inside beads, whereas in coated samples they mostly occur outside beads. The difference in behavior is in agreement with the pullout tests, in which the fiber tends to pull out from an uncoated bead, whereas it remains bonded to the bead in coated samples.

When the bead-matrix friction is low (for example, by coating), the bead slope efficiently converts the pullout stress into a radial stress which enhances the gripping of the fiber by the bead, an action similar to that of an inclined wedge (see discussion on the bead locking mechanism). As a result, the fiber does not break prematurely inside the bead, and the coated bead absorbs energy by pushing through the matrix.

3.4. Crack propagation - compact tension tests

Preliminary compact tension tests (Fig. 10a) of beadless and uncoated beaded fibers laid down perpendicular to a propagating

crack demonstrate the role and contribution of beads to the slowing down of crack propagation by fiber bridging. Beaded fibers appear to remain intact for some time after the crack tip crosses a fiber (Fig. 10b), as well as delay fiber-matrix debonding, implying bridging across the crack due to anchoring by the beads (as demonstrated in the Supporting Information compact tension video). By comparison, beadless fibers tend to debond and break before the crack tip reaches the fiber (Fig. 10c). Generally, this behavior is in agreement with the known Cook-Gordon mechanism for crack propagation in brittle systems [44], which predicts that the stress field ahead of the crack tip can initiate a secondary crack in a weak interface normal to the crack surface, delaying the primary crack. Such delaying effect seems more pronounced in the case of beaded fibers (see video).

Supplementary video related to this article can be found at <https://doi.org/10.1016/j.compscitech.2018.03.003>.

3.5. Bead locking mechanism

The mechanical locking mechanism of the fiber-bead-matrix

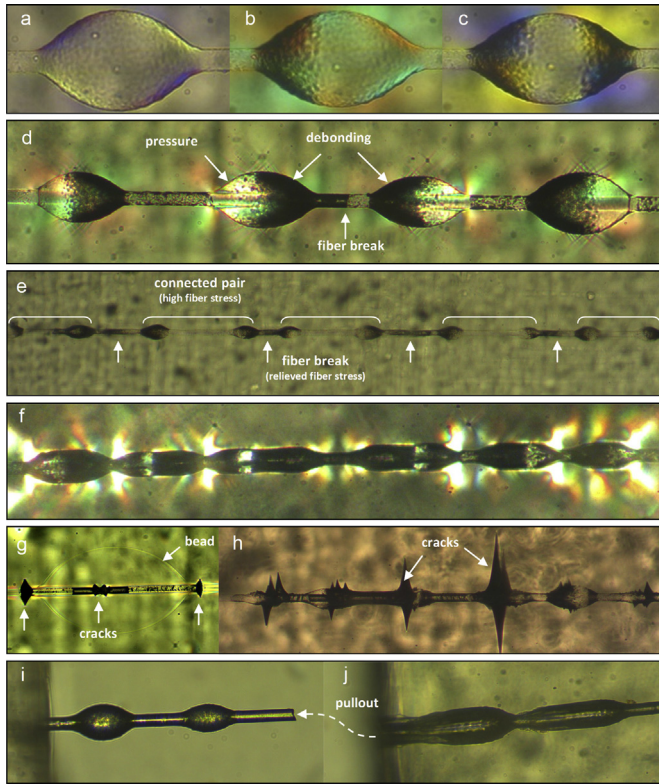


Fig. 9. Polarized OM images of beaded-fiber fragmentation specimens. 18 μm E-glass fibers with coated EP-828 epoxy beads. (a) Stress on a bead prior to debonding, (b) after partial debonding (dark area on left face), and (c) after almost complete debonding. (d) Debonding of a string of beads followed by fiber breakage (at center), and beads pushing against the matrix in opposite directions (brighter regions). (e) Recurrent pairs of beads connected by fiber under tension (clearer fiber segments, marked by arcs) following fiber debondings (darker fiber segments) and breakages (marked by arrows). (f) Beads pulled in opposite directions against the matrix (brighter regions), accompanied by extensive plastic deformation (oblong voids) of the matrix. (g) Initiation of cracks inside and outside a bead. (h) Cracks associated with beads. (i) Beaded fiber pulled out following matrix fracture, (j) leaving oblong cavities.

system is an interplay between geometry, material and friction features. These include the bead size and shape, fiber diameter, material and interfacial strength of each component, and friction coefficients. In principle, initial failure under external load can occur in any of the structural components - fiber, matrix or bead - and in any of the interfaces - fiber-bead, fiber-matrix or bead-matrix. The weakest link is determined by the specific combination of the components' geometries, materials and interfaces in a given case. These complex relationships are briefly discussed here, in light of the trends observed in the experiments. A complete theoretical model of the bead locking mechanism is beyond the scope of this article.

The bead acts much like an inclined wedge pressed between two components, in our case the matrix and the fiber (Fig. 11). When a longitudinal pullout stress σ_F is applied on the fiber, the fiber pulls the bead against the matrix, resulting in two stress components at the bead-matrix interface, longitudinal and radial. The magnitude of the radial stress component depends on the bead-matrix interfacial friction μ and slope θ , such that when the friction is reduced (for example, by coating) the radial stress can increase significantly. Thus, high values of μ may represent the uncoated condition and a static interface, whereas low values may represent the coated condition and a sliding interface, and transition from the first condition to the second may happen if interfacial debonding occurs during loading. The rigid fiber reacts

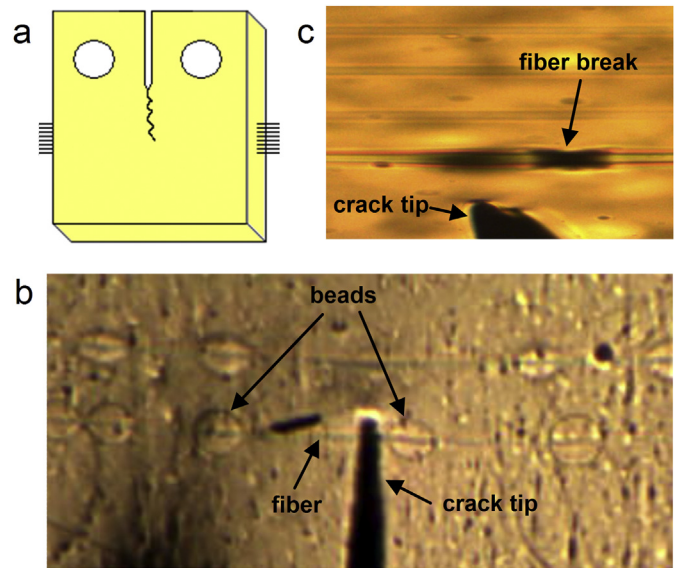


Fig. 10. OM images of crack propagation in fiber-reinforced epoxy. Four 18 μm E-glass fibers. (a) Compact tension notched specimen (see details in Ref. [45]), drawn by Minimat at rate of 0.05 mm/min. (b) Fibers with uncoated EP-828 epoxy beads. (c) Beadless fibers.

with an opposite radial stress, which generates a friction stress (in shear) that enhances the effective fiber-bead interfacial strength. Under certain conditions, specifically low μ and low θ , this stress may even lead to a friction-lock state that precludes fiber pullout from the bead. This 'fiber gripping' effect agrees well with our experimental observations, which demonstrated that the fiber-bead adhesion tends to be stronger in the coated samples compared to the uncoated ones, resulting in a higher pullout force (Fig. 8).

Why does the bead not yield under pull-out and fragmentation, whereas the matrix does, even though both are made of the same material? The radial stress between the bead and the matrix has the effect of contracting the bead while expanding the matrix, and therefore the bead and matrix incur also circumferential stresses, similar in magnitude but compressive in the bead while tensile in the matrix. The elastic distortion energy due to the combination of the two orthogonal stresses, radial and circumferential, is always higher in the matrix than in the bead, as both are compressive in the case of the bead, whereas they are compressive and tensile in the case of the matrix (von Mises yield criterion). This clarifies why, in the pullout and fragmentation tests (Figs. 7 and 9), the bead did not yield even when the matrix yielded. This favorable stress condition for the bead, together with the fiber gripping effect, make the intermittent beading concept viable.

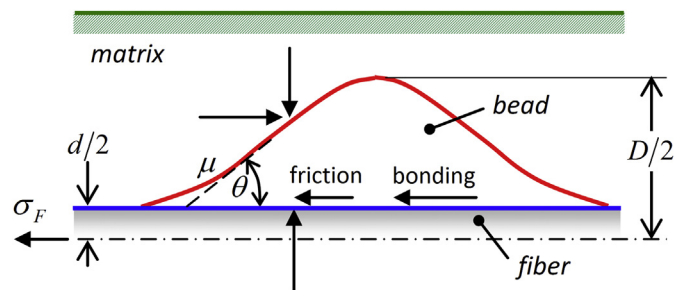


Fig. 11. Stresses acting on a bead. The stresses are denoted by thick arrows. σ_F is an external load applied on the fiber. μ is the bead-matrix friction coefficient and θ is the bead slope angle (marked by a dashed line).

Three different failure mechanisms or domains are possible, depending on the stresses that develop in the matrix, fiber-bead and fiber-matrix interfaces and fiber, and whether they exceed the strength of any of these components, σ_m , τ_i and σ_f , respectively. Evidently, failure would initiate in the component whose strength is exceeded first. For example, by reducing the bead-matrix friction, fiber gripping could be enhanced because the radial stress in the bead is higher (as explained above), and consequently the matrix could eventually yield (σ_m is exceeded) under the bead pressure, preempting fiber-bead debonding (τ_i is not exceeded). Such a transition in failure mechanism was indeed observed in the pullout tests, where in the samples with release-agent coating the fiber and bead typically pulled out together from the matrix (Fig. 7b and e), following matrix yield, whereas in the uncoated samples the fiber pulled out from the bead (Fig. 7a and d).

The pullout work of a beaded fiber is basically insensitive to fiber-bead and bead-matrix debonding, because, in addition to dissipating debonding energy as in beadless fibers, a beaded fiber absorbs energy by plastically deforming the matrix. It appears from the set of experiments performed here that beaded fibers provide better toughness performance compared to beadless fibers, for a given set of material properties. In other words, it is a structural obstacle toughening effect.

The same epoxy was used for both the bead and matrix in the current basic study, and therefore their mechanical properties were similar, except possibly for a minor difference due to the longer curing time to which the bead was exposed. When a cured beaded fiber is embedded in a curing matrix, the latter forms bonds with the bead surface. Although this bonding is epoxy to epoxy, the interface does not disappear. Indeed, the bonding structure and properties are different from those of bulk epoxy as clearly evidenced in the higher force necessary to pull out the beaded fibers (FB) compared to the pullout force of beadless fibers (F), seen in Fig. 8a. Notwithstanding, different bead and matrix materials and bonding can be selected (possibly in an empirical way) in order to achieve a desired effect.

3.6. Critical length and composite performance

We now address the issue of how the critical length and structural strength and toughness are affected in a composite reinforced by beaded fibers. In particular, we question whether the classical

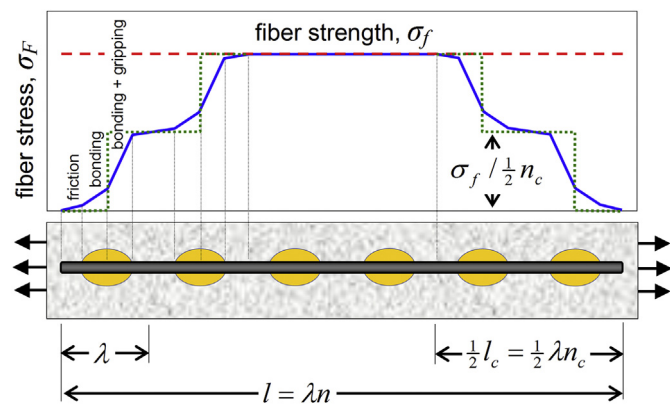


Fig. 12. Illustration of fiber stress and critical length in a beaded fiber. The fiber stress gradually rises from its ends toward the center (blue solid curve), and is also approximated by discrete steps (green dotted curve). The contributions to fiber stress are indicated: fiber-matrix friction (after debonding), fiber-bead bonding, and fiber-bead bonding + gripping. In this illustration, the number of fiber beads is $n = 6$ and the critical number of beads is $n_c = 4$. (For interpretation of the references to color in this figure legend, the reader is referred to the Web version of this article.)

concept of critical length still has a meaning similar to that for beadless fibers, and whether it can still be used as an indication of the quality of interfacial adhesion. We show that, in the case of beaded fibers, the maximum fiber stress is determined predominantly by the number of beads on the fiber rather than by the fiber length. Specifically, we define a new notion of critical number of beads n_c , a discrete quantity, to replace the classical notion of critical length l_c , a continuous quantity. We show that n_c reflects the structural strength of the bead locking mechanism, dominated not by adhesion but by the complex geometry and strength of the fiber-bead-matrix system. We further show how the composite strength and toughness are affected by n_c .

Under external load, the fiber stress builds up by contributions from the bead-matrix interface and from the fiber-matrix interface (in fiber sections not covered by a bead). However, the fragmentation test demonstrated that interfacial debonding of these interfaces tends to occur first, followed by pressure exerted by the beads on the matrix and eventually matrix yielding. In that sense, there no difference between the coated and uncoated cases, so long as such debonding occurs. At that stage, the shear stress in the matrix bonded interfaces is mostly relieved due to debonding, and therefore the dominant contribution to fiber stress comes from the beads. Each bead contributes a (close to) step jump in the stress, as most of the contribution is concentrated in the relatively short region where fiber gripping is strong, as illustrated in Fig. 12.

We observe that most fiber breaks occur between beads at regular spacing, such that the number of beads between fiber fractures is fairly constant, as seen in the latest steps of the fragmentation test (close to saturation limit) (Fig. 9e and h). In other words, there exists a critical number of beads, n_c , above which, under load, the fiber stress exceeds its strength σ_f (see Fig. 12). n_c is likely to be an even number ≥ 2 (2,4,6,8, ...), because, with an odd number of beads, the bead at the fragment center does not bear load, as it cannot press against the matrix from both its opposite faces. This is clearly seen in Fig. 9d–f, where pressure on the matrix (bright regions) is applied only from one side of a bead, while the stress in the opposite side is relieved. The critical number of beads n_c can be derived experimentally from the measured average number of beads in fiber fragments in a fragmentation test, in a manner similar to the measurement of critical length in beadless fibers [13,17,18].

The concept of a critical number of beads n_c in beaded fibers is analogous to the concept of a critical length l_c in beadless fibers, for which $l_c = \sigma_f D / 2\tau_i$. The length of a fiber with n beads is $l = \lambda n$, and thus, its critical length can be expressed by $l_c = \lambda n_c$, where l and l_c are lengths that correspond to the discrete values of n and n_c , respectively. The shortest possible critical length of a beaded fiber is $l_c = 2\lambda$, when $n_c = 2$, in other words a fiber having a single bead on each edge. Finally, the useful ratio l/l_c is equal to n/n_c . This analogy is illustrated in Fig. 12.

When a crack develops in a composite under load, beaded fibers having embedded sections with more than $n_c/2$ beads from both sides of the crack surface will break, contributing a stress σ_f each, whereas those embedded sections having less beads (randomly distributed between 0 and $n_c/2$) will pull out, contributing an average stress $\sigma_f/2$ each. For long fibers having n beads each, the fraction of fibers that pull out is n_c/n , whereas the fraction of fibers that break is $1 - n_c/n$. Thus, the sum contribution of the broken and pulled out fiber sections, weighted by their respective fraction, to the composite strength is approximately given by:

$$\sigma_b \approx V_f \sigma_f \left(1 - \frac{1}{2n/n_c} \right) \quad (1)$$

(depicted in Fig. 13a) where V_f is the fiber volume fraction in the

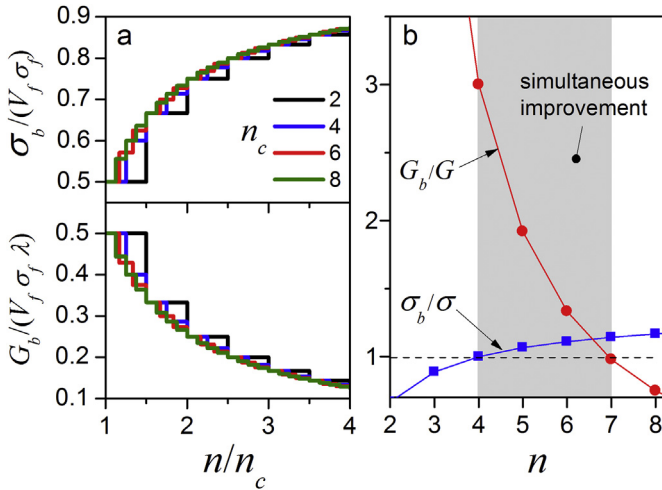


Fig. 13. Beaded composite strength and toughness. (a) Normalized composite strength $\sigma_b/(V_f\sigma_f)$ and toughness $G_b/(V_f\sigma_f\lambda)$ vs. the relative number of beads. n is the number of beads in a fiber, n_c is the critical number of beads, λ is the (average) distance between beads, V_f is the fiber volume fraction, and σ_f is the matrix strength. (b) Region of simultaneous strength and toughness improvement of beaded fibers ($n_c = 2$) with respect to beadless fibers of the same length ($l/l_c = 2$). See the example detailed in the text.

composite. This expression is analogous to the CKT model for beadless fibers, when substituting n/n_c by l/l_c . It demonstrates that when using beaded fibers, the composite strength increases with the number of beads. In other words, if $n/n_c = l/l_c$, the strength behavior of beaded and beadless fibers is similar. However, it is known that for regular (beadless) fibers, the composite strength predicted by CKT can be degraded by nonuniform shear stress distribution and poor bonding quality [38,46]. By contrast, with beaded fibers the strength is not sensitive to interfacial uniformity or quality, as the contribution of each bead to the overall strength is achieved by mechanical locking instead of shear. This provides a potential advantage to composites made of beaded fibers.

To estimate the composite toughness, we consider the energy absorbed by pullout of beaded fibers through the fracture plane of a crack, as observed in Fig. 9i and j. Assuming beads of equal diameter, each bead dissipates energy by displacing the matrix only over a pullout length of about λ , as the preceding beads already displaced the matrix in its pullout path (Fig. 9f and j). The maximum stress in a pulled out fiber section varies between 0 and σ_f , as a higher stress will result in fiber breakage which dissipates little energy. Thus, for a fiber having a cross sectional area a , the average pullout force is $1/2\sigma_f a$, and the corresponding pullout energy is $1/2\sigma_f a\lambda$. The number of fibers per unit area crossing the fracture plane is V_f/a , but only a fraction n_c/n of these fibers will have a

short embedded section that can be pulled out. Put together, the total pullout energy per unit area of the fracture plane is approximately given by:

$$G_b \approx \frac{V_f\sigma_f\lambda}{2n/n_c} \quad (2)$$

as depicted in Fig. 13a. Thus, less beads (relatively) would appear to be better for toughness but worse for strength, and vice versa.

By comparison, the toughness for beadless fibers is $G = 1/12V_f\sigma_f l_c^2/l$ when the CKT model is assumed [13]. Substituting $l = \lambda n$ and $l_c = \lambda n_c$ in G for the purpose of comparison with G_b , we get $G_b/G \approx 6/n_c$. This means that whenever a beaded fiber has a critical number of beads $n_c < 6$, a composite reinforced by such fibers should have higher toughness compared to a composite reinforced with beadless fibers of the same length, critical length, volume fraction and strength. This somewhat surprising result reflects that different energy absorption mechanisms are at play: in beadless fibers, the pullout stress decreases from its maximum value linearly with the pullout travel distance, whereas in beaded fibers the pullout stress remains constant at its maximum value for a travel distance of λ , then drops sharply to a low value. Consequently, n_c cannot simply replace l_c in the CKT toughness model.

The following example may clarify under which conditions strength and toughness improvements can simultaneously be achieved in beaded fibers relative to beadless fibers of the same length, strength and volume fraction. Starting with beadless fibers having a given l/l_c , we can apply beads at a desired size and frequency to these fibers such that the condition $n/n_c = l/l_c$ is met, and therefore the strength of both composites is the same (equation (1)). Provided that the beads are chosen so that $n_c = 2$, the toughness of the beaded composite will be higher than that of the beadless composite by a factor $G_b/G \approx 3$ as shown above (equation (2)). Thus, under this condition, the toughness is greatly improved, with no harm to the strength. We then gradually increase the number of beads n , without modifying the beads size in order to retain the value of n_c . By doing so, the relative strength improvement progressively rises, at the expense of some reduction in the relative toughness improvement. These trends are demonstrated in Fig. 13b, which shows the existence of a region of simultaneous improvement.

Note that the CKT-based classical expression for G assumes perfect plasticity (that is, indefinite strain at a constant shear yield stress), a condition that rarely exists in polymer composites [38], and therefore the value of G should be degraded significantly as a result of debonding. Reinforcement with beaded fibers is not as sensitive to debonding, a significant advantage.

As seen above, the composite strength and toughness are both linearly dependent on the fiber volume fraction V_f , the maximum of which is achieved when the fibers are tightly packed. Two tight

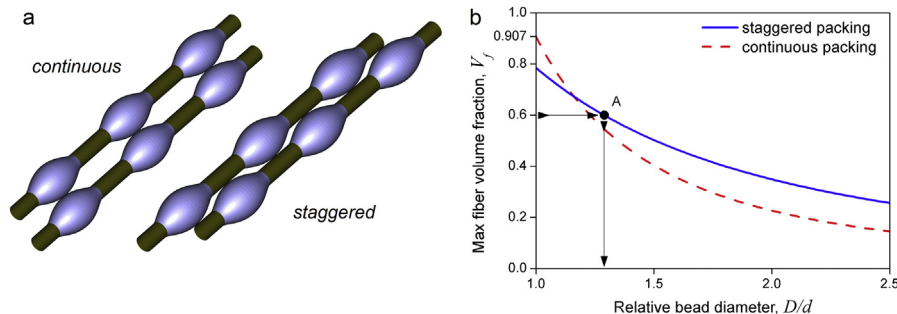


Fig. 14. Beaded fibers tight packing. (a) Continuous and staggered packing structures. (b) Maximum achievable volume fraction vs. relative bead diameter.

packing structures are possible with beaded fibers: (i) continuous packing, where each bead is in contact with six neighboring beads, and (ii) staggered packing, where each bead is in contact with four neighboring fibers (Fig. 14a). In staggered packing, fibers are shifted longitudinally by half a bead wavelength with respect to their contacting neighbors, providing tighter packing compared to continuous packing. The maximum achievable volume fraction with beaded fibers is bounded by the bead diameter, as depicted in Fig. 14b (see calculation in Supporting Information S4). Due to statistical dispersion of the beads wavelength, the actual V_f would lie between the curves of the two packing structures. Obviously, when high volume fraction is desired, the bead diameter should be relatively small, as exemplified by point A in Fig. 14b for 60% volume fraction. However, a small bead should be effective in tight staggered packing because the mechanical locking mechanism would be based on bead-to-bead interaction, instead of the bead-to-matrix interaction for looser packing, somewhat reminiscent of the interlocking in dovetailed platelets of nacre [35].

4. Conclusions

Under certain conditions, intermittent beading holds the potential for achieving simultaneous improvement of strength and toughness in composite materials. By tuning the beads size and shape (Supporting Information S2-S3) and the bead-matrix friction, the composite strength and toughness can in principle be controlled to a wider range than possible with beadless fibers. In the current study, we limited ourselves to the contact angle resulting from the natural surface tensions of the liquid epoxy resin and glass fiber, but selection of solvents, surface treatments, and even the surrounding medium around the bead (gaseous or liquid) may allow broader diversity.

As demonstrated both experimentally and theoretically here, beaded fibers function as geometrical 'locks' through compressive and tensile stresses rather than shear. As a consequence, with beaded fibers the composite mechanical performance is not as sensitive to bonding quality or uniformity as with beadless fibers. In other words, beads as structural obstacles appear to be more efficient as toughening agents than interfacial chemical tuning. When high fiber volume fraction is desired, the beads should be small and the beaded fibers tightly packed and staggered, resulting in bead-to-bead interaction instead of bead-to-matrix, with a dovetail-like interlocking action.

Intermittent beading is not limited to unidirectional long fibers, the model used here to demonstrate the underlying basic principles of the fiber-bead-matrix system. The concept offers a wide design flexibility by tuning geometry, materials, interfaces, fibers alignment, and even intermixture of features (hybridization) in a composite, to meet specific requirements. Further work is anticipated in addressing open questions and expanding the scope to a wider variety of fiber, matrix and bead materials, surface treatments and geometries, and to other size scales. Intermittent beading can be applied during fiber processing, and its implementation in composite reinforcement has ample possibilities for optimization.

Acknowledgements

The authors would like to acknowledge partial support from the G.M.J. Schmidt Minerva Centre of Supramolecular Architectures at the Weizmann Institute, and the China-Israel Science Foundations collaborative research grant 3322/12. This research was also made possible in part by the generosity of the Harold Perlman family. H.D.W. is the recipient of the Livio Norzi Professorial Chair in Materials Science. Acknowledgement is due to Dr. Ing. Gerhard Kalinka from Bundesanstalt für Materialforschung und -prüfung (BAM),

Berlin, Germany for his help in building the pullout device and its control software.

Appendix A. Supplementary data

Supplementary data related to this article can be found at <https://doi.org/10.1016/j.compscitech.2018.03.003>.

References

- [1] B. Harris, W.R. Beaumont, E. Moncunil, Strength and fracture toughness of carbon fibre polyester composites, *J. Mater. Sci.* 6 (3) (1971), 238–&.
- [2] H.C. Tsai, A.M. Arocho, L.W. Gause, Prediction of fiber matrix interphase properties and their influence on interface stress, displacement and fracture-toughness of composite-material, *Mater. Sci. Eng., A Struct. Mater. Prop. Microst. Process.* 126 (1990) 295–304.
- [3] M. Tanoglu, S.H. McKnight, G.R. Palmese, J.W. Gillespie, The effects of glass-fiber sizings on the strength and energy absorption of the fiber/matrix interphase under high loading rates, *Compos. Sci. Technol.* 61 (2) (2001) 205–220.
- [4] R.O. Ritchie, The conflicts between strength and toughness, *Nat. Mater.* 10 (11) (2011) 817–822.
- [5] M.F. Ashby, *Materials Selection in Mechanical Design*, fourth ed., Butterworth-Heinemann, 2010.
- [6] L. Yang, I. Greenfeld, H.D. Wagner, Toughness of carbon nanotubes conforms to classic fracture mechanics, *Sci. Adv.* 2 (2) (2016).
- [7] I. Greenfeld, X.M. Sui, H.D. Wagner, Stiffness, strength, and toughness of electrospun nanofibers: effect of flow-induced molecular orientation, *Macromolecules* 49 (17) (2016) 6518–6530.
- [8] X.M. Sui, H.D. Wagner, Tough nanocomposites: the role of carbon nanotube type, *Nano Lett.* 9 (4) (2009) 1423–1426.
- [9] X.M. Sui, E. Wiesel, H.D. Wagner, Enhanced mechanical properties of electrospun nano-fibers through NaCl mediation, *J. Nanosci. Nanotechnol.* 11 (9) (2011) 7931–7936.
- [10] F. Barthelat, Z. Yin, M.J. Buehler, Structure and mechanics of interfaces in biological materials, *Nat Rev Mater* 1 (4) (2016).
- [11] S. Weiner, H.D. Wagner, The material bone: structure-mechanical function relations, *Annu. Rev. Mater. Sci.* 28 (1) (1998) 271–298.
- [12] U.G.K. Wegst, H. Bai, E. Saiz, A.P. Tomsia, R.O. Ritchie, Bioinspired structural materials, *Nat. Mater.* 14 (1) (2015) 23–36.
- [13] I. Greenfeld, H.D. Wagner, Nanocomposite toughness, strength and stiffness - the role of filler geometry, *Nanocomposites* 1 (2015) 3–17.
- [14] X.M. Sui, I. Greenfeld, H. Cohen, X.H. Zhang, Q.W. Li, H.D. Wagner, Multilevel composite using carbon nanotube fibers (CNTF), *Compos. Sci. Technol.* 137 (2016) 35–43.
- [15] S.K. Khanna, A. Shukla, Energy-absorption mechanisms during dynamic fracturing of fiber-reinforced composites, *J. Mater. Sci.* 28 (14) (1993) 3722–3730.
- [16] A.G. Evans, Perspective on the development of high-toughness ceramics, *J. Am. Ceram. Soc.* 73 (2) (1990) 187–206.
- [17] A.H. Cottrell, Strong solids, *Proc. Roy. Soc. Lond. A* 282 (1964).
- [18] A. Kelly, W.R. Tyson, Tensile properties of fibre-reinforced metals - copper/tungsten and copper/molybdenum, *J. Mech. Phys. Solid.* 13 (6) (1965), 329–&.
- [19] A. Kelly, Interface effects and work of fracture of a fibrous composite, *Proc. Roy. Soc. Lond. Math. Phys. Sci.* 319 (1536) (1970), 95–&.
- [20] A.G. Atkins, Imparting strength and toughness to brittle composites, *Nature* 252 (5479) (1974) 116–118.
- [21] A.G. Atkins, Intermittent bonding for high toughness - high-strength composites, *J. Mater. Sci.* 10 (5) (1975) 819–832.
- [22] R.E. Jensen, S.H. McKnight, Inorganic-organic fiber sizings for enhanced energy absorption in glass fiber-reinforced composites intended for structural applications, *Compos. Sci. Technol.* 66 (3–4) (2006) 509–521.
- [23] X. Gao, R.E. Jensen, S.H. McKnight, J.W. Gillespie, Effect of colloidal silica on the strength and energy absorption of glass fiber/epoxy interphases, *Compos. Appl. Sci. Manuf.* 42 (11) (2011) 1738–1747.
- [24] N. Phanhtien, Effective elastic-moduli of enlarged-end-fiber-reinforced solids, *Fibre Sci. Technol.* 14 (4) (1981) 241–250.
- [25] N. Phanhtien, On the pull-out of fibers with enlarged ends, *Fibre Sci. Technol.* 15 (2) (1981) 111–116.
- [26] Y.T. Zhu, J.A. Valdez, N. Shi, M.L. Lovato, M.G. Stout, S.J. Zhou, D.P. Butt, W.R. Blumenthal, T.C. Lowe, A composite reinforced with bone-shaped short fibers, *Scripta Mater.* 38 (9) (1998) 1321–1325.
- [27] Y.T. Zhu, J.A. Valdez, I.J. Beyerlein, S.J. Zhou, C. Liu, M.G. Stout, D.P. Butt, T.C. Lowe, Mechanical properties of bone-shaped-short-fiber reinforced composites, *Acta Mater.* 47 (6) (1999) 1767–1781.
- [28] Y.T. Zhu, I.J. Beyerlein, J.A. Valdez, T.C. Lowe, Fracture toughness of a composite reinforced with bone-shaped short fibers, *Mater. Sci. Eng., A Struct. Mater. Prop. Microst. Process.* 317 (1–2) (2001) 93–100.
- [29] I.J. Beyerlein, Y.T. Zhu, S. Mahesh, On the influence of fiber shape in bone-shaped short-fiber composites, *Compos. Sci. Technol.* 61 (10) (2001) 1341–1357.
- [30] Y.T. Zhu, I.J. Beyerlein, Bone-shaped short fiber composites - an overview,

- Mater. Sci. Eng., A Struct. Mater. Prop. Microst. Process. 326 (2) (2002) 208–227.
- [31] R.C. Wetherhold, F.K. Lee, Shaped ductile fibers to improve the toughness of epoxy-matrix composites, *Compos. Sci. Technol.* 61 (4) (2001) 517–530.
- [32] R.M. Bagwell, R.C. Wetherhold, Improvement in fracture toughness of an epoxy/copper composite through the use of various end shaped fibers, *Mater. Sci. Eng., A Struct. Mater. Prop. Microst. Process.* 361 (1–2) (2003) 294–301.
- [33] R.M. Bagwell, R.C. Wetherhold, Fiber pullout behavior and impact toughness of short shaped copper fibers in thermoset matrices, *Compos. Appl. Sci. Manuf.* 36 (5) (2005) 683–690.
- [34] R.C. Wetherhold, M. Corjon, P.K. Das, Multiscale considerations for interface engineering to improve fracture toughness of ductile fiber/thermoset matrix composites, *Compos. Sci. Technol.* 67 (11–12) (2007) 2428–2437.
- [35] F. Barthelat, H.D. Espinosa, An experimental investigation of deformation and fracture of nacre-mother of pearl, *Exp. Mech.* 47 (3) (2007) 311–324.
- [36] J.J. Blaker, D.B. Anthony, G. Tang, S.R. Shamsuddin, G. Kalinka, M. Weinrich, A. Abdolvand, M.S.P. Shaffer, A. Bismarck, Property and shape modulation of carbon fibers using lasers, *ACS Appl Mater Inter* 8 (25) (2016) 16351–16358.
- [37] C.T. Chou, U. Gaur, B. Miller, The effect of microvoid gap width on microbond pull-out test-results, *Compos. Sci. Technol.* 51 (1) (1994) 111–116.
- [38] M. Piggott, *Load Bearing Fibre Composites*, second ed., Kluwer Academic Publishers, 2002.
- [39] W. Zhang, J. Duchet, J.F. Gerard, Self-healable interfaces based on thermo-reversible Diels-Alder reactions in carbon fiber reinforced composites, *J. Colloid Interface Sci.* 430 (2014) 61–68.
- [40] P.G. de Gennes, F. Brochard-Wyart, D. Quere, *Capillarity and Wetting Phenomena - Drops, Bubbles, Pearls, Waves*, Springer-Verlag New York, Inc, 2004.
- [41] J. Plateau, *Statique experimentale et theorique des liquides soumis aux seules forces moleculaires* (Experimental and theoretical equilibrium state of liquids subjected to molecular forces only), Gauthiers-Villars, Paris, 1873.
- [42] L. Rayleigh, *Scientific Papers*, (Cambridge: Cambridge University Press, 1899): *Proc. London Math. Soc.* 10, 4 (1878); *Proc. R. Soc. London* 29, 71(1879); *Philos. Mag.* 34, 145 (1873).
- [43] S. Haefner, M. Benzaquen, O. Baumchen, T. Salez, R. Peters, J.D. McGraw, K. Jacobs, E. Raphael, K. Dalnoki-Veress, Influence of slip on the Plateau-Rayleigh instability on a fibre, *Nat. Commun.* 6 (2015).
- [44] J. Cook, J.E. Gordon, C.C. Evans, D.M. Marsh, A mechanism for the control of crack propagation in all-Brittle systems, *Proc. Roy. Soc. Lond. Math. Phys. Sci.* 282 (1391) (1964).
- [45] N. Lachman, H.D. Wagner, Correlation between interfacial molecular structure and mechanics in CNT/epoxy nano-composites, *Compos. Appl. Sci. Manuf.* 41 (9) (2010) 1093–1098.
- [46] H.L. Cox, The elasticity and strength of paper and other fibrous materials, *Br. J. Appl. Phys.* 3 (1952) 72.